Journal of *Marine Science and Engineering*

MDPI

Article

A Jacket-Frame Mounted Oscillating Water Column with a Variable Aperture Skirt

Carlos Pérez-Collazo [1,*], Deborah M. Greaves [2] and Gregorio Iglesias [2,3]

[1] Centro Universitario de la Defensa en la Escuela Naval Militar, Plaza de España s/n, 36920 Marín, Spain
[2] School of Engineering, Computing and Mathematics, University of Plymouth, Plymouth PL4 7AA, UK
[3] MaREI Centre, Environmental Research Institute & School of Engineering, University College Cork, T12AK5 Cork, Ireland
* Correspondence: carlos.perez.collazo@cud.uvigo.es

Abstract: During the last decade jacket-frames have emerged as the main kind of substructure for bottom-mounted offshore wind farms in intermediate water depths. With the offshore wind industry moving towards deeper waters, the predominance of jacket-frames is expected to increase in future years. Multipurpose platforms combining wind and wave energy are proposed as an innovative solution to enhance the sustainability of offshore wind energy. In this research, a multipurpose platform is investigated with a novel feature in its oscillating water column (OWC) wave energy converter—a variable geometry skirt. A comprehensive physical modelling campaign was carried out using a 1:50 scale model. The performance of the OWC and its interaction with the wave field were investigated under four different skirt aperture angles. It was found that the skirt aperture angle plays a significant role in the capture-width ratio and the pneumatic mean power of the OWC. The best performance was obtained with a skirt aperture angle of 140 deg. More generally, these results prove that the variable-geometry skirt is a promising innovation for hybrid wave-wind systems mounted on jacket-frame substructures.

Keywords: hybrid wind-wave energy; oscillating water column (OWC); offshore wind; physical modelling

Citation: Pérez-Collazo, C.; Greaves, D.M.; Iglesias, G. A Jacket-Frame Mounted Oscillating Water Column with a Variable Aperture Skirt. *J. Mar. Sci. Eng.* **2023**, *11*, 2383. https://doi.org/10.3390/jmse11122383

Academic Editors: Pedro Beirão and Mário J. G. C. Mendes

Received: 4 November 2023
Revised: 15 December 2023
Accepted: 15 December 2023
Published: 18 December 2023

1. Introduction

In the global effort towards mitigating climate change [1], the adoption of a clean energy system based on harnessing renewable energy resources is fundamental [2]. These efforts have seen exceptional development in the offshore wind industry in recent years [3]. However, if the ambitious objectives of the Paris Agreement [4] are to be achieved, to keep global temperature rise this century below 2 degrees Celsius above pre-industrial levels, the European offshore wind industry should fulfil its ambition of installing 460 GW by 2050 [5].

To foster offshore wind energy while maintain its low impact on other marine resources, it is important to consider its multiuse, combining exploitation with other marine resources such as wave energy [6], aquaculture, seaweed farming [7], and maritime leisure [8]. It is in relation to this and on the various synergies that offshore wind energy and wave energy conversion systems have that the combination of those technologies was proposed [9–11]. Among these synergies, it is worth remarking the increased sustainability that the combined exploitation of two marine resources would have in comparison with independent offshore wind and wave energy projects. This is not only justified for the shared costs due to the combined access to common infrastructures and facilities, but also for the lower seabed footprint of a combined project [9,12]. Increasing the energy yield per area of seabed used is a key parameter to reduce pressure on conventional marine recourses users, such as fisheries [13]. Therefore, combined multiuse energy platforms are expected to contribute to accelerate the deployment of offshore renewable energies and, at

the same time, ensure the sustainability of multiple maritime sectors and their respective economic activities.

Previous research on hybrid systems was initially led by some EU funded research projects, including MARINA Platform [14], MERMAID [15], and ORECCA [16]. These projects led to the definition of several hybrid concepts during the last decade. Dong et al. [17] have recently identified more than 39 different hybrid concepts that were proposed to date. Out of these, 27 combined an oscillating body (OB) type of wave energy converter (WEC) into the foundation system of an offshore wind turbine (e.g., [18–21]), while 12 utilised an oscillating water column (OWC) type of WEC (e.g., [22–28]). When it comes to the integration of Wind-OWC (W-OWC) hybrid concepts into intermediate waters offshore wind foundation systems [9], with typically greater than 30–40 m water depth, the jacket-frame substructure is most commonly considered [29,30]. However, jacket-frame substructures are among the most expensive to manufacture; they have a higher load capacity combined with a reduced seabed impact and a larger water depth range of installation (up to 80 m in recent projects) [31,32]. This has raised them among the most common substructure types for these water depth ranges. With the offshore wind industry pushing forward towards deeper water grounds and targeting intermediate and deep-water projects, jacket-frame and floating substructures are the ones expected to pay a leading role in the next couple of decades. This makes jacket-frame substructures a clear candidate when considering a hybrid wind-wave energy system.

Among WEC technologies, OWCs are considered one of the most successful options, partially due to the simplicity of the concept. These are formed by a hollow chamber partially submerged in water with an open bottom and a trapped air volume, which is driven in and out of the chamber through an air turbine by the action of the incoming waves, and also for their low operational and maintenance costs [33]. When it comes to increasing performance of an OWC, it is important to address the air turbine part of the system, as evidenced by the fact that multiple air turbine designs have been investigated in the last few decades, mostly self-rectifying air turbines [34]. The hydrodynamics of the OWC chamber is also known to have a relevant effect on the overall system performance; chambers should be designed to ensure a near-resonant condition for the incident waves while at the same time avoiding energy losses [35,36].

The effects on the OWC geometry on its performance have been widely investigated in previous literature. Boccotti [37] compared the effect of the front wall on an U-OWC with a conventional OWC, finding an increase in the natural period of oscillation. Rezanejad et al. [38] proposed the addition of a step at the front of the OWC chamber, increasing, in this way, an additional resonant mechanism close to the frequency of the incident waves. An L-shaped OWC geometry oriented in the wave propagation direction was proposed by [39,40]. Furthermore, several publications have tackled the effects that specific geometrical variations would have on the performance, for example, effects of the length and the opening angle of harbour walls [41] and the slope of the chamber's front and rear walls [42]. In addition, when it comes to isolated OWC devices, cylindrical chambers are the most often used, so that the wave direction does not affect performance [43], as has been studied for nearshore sites [44,45]. It is in relation to this that the work preceding this publication has proposed a patent application [46] of a variable geometry OWC chamber to be installed as a hybrid wind-wave energy system. Among the different systems proposed in such patent application, there is one proposing a variable aperture skirt, which aims to increase the energy performance of the OWC by orienting the skirt aperture to the incident wave direction.

The work presented in this paper aims to further understand the hydrodynamic response of a jacket-frame mounted OWC (Figure 1), which has a novel skirt system that can adjust its geometry to different aperture angles. This research explores a variable aperture skirt system that extends the hybrid wind-wave energy converter previously introduced in [47]. A thorough test campaign involving a 1:50 scale model of this device was carried out, considering various skirt setups. Following this experimental campaign,

the interaction between the OWC skirt aperture and the wave field was studied. The performance of the different skirt aperture angles was assessed and compared with the previous research.

Figure 1. Jacket-frame mounted OWC energy converter (partially reproduced from [47]).

The remaining content of this article has been structured as follows. Section 2 outlines the materials and methods employed in the experimental campaign. Section 3 details the results derived from this campaign, subsequently analysed in Section 4. Ultimately, Section 5 draws conclusions based on the findings.

2. Materials and Methods

2.1. The Model

The physical model used for this research (Figure 2) was built upon that used in [47]. Four different OWC configurations were considered, comprising an individual OWC chamber configuration for each skirt aperture angle. Figure 3 and Table 1 outline the key dimensions and parameters of the jacket-frame foundation, the OWC chamber, and its skirt. Furthermore, the scale model was targeted for a site with a 50-m water depth [43]; geometrical similarity and Froude dynamic similitude criterion were considered for the part of the chamber of the OWC below the mean free surface [48]. The Froude number (Fr) is defined as the ratio between inertia (F_i) and gravity forces (F_g):

$$F_r = \frac{F_i}{F_g} = \frac{v^2}{g\,L}, \tag{1}$$

where, v is a characteristic velocity of the system, g is the gravitational acceleration, and L is a characteristic length of the system.

Air compression forces have a significant role in an OWC system, and this requires a different scaling of the pneumatic section of the chamber, the OWC chamber above the still water level, to account for the air compressibility effects [49,50]. Hence, for this experiment the volume of the pneumatic part of the chamber was scaled using scale ratio equal to λ^2, instead of the λ^3 suggested by Froude, following [51–53]—i.e., this means that the volume of the air part of the OWC chamber should be oversized, in comparison with a Froude geometrical scaled model.

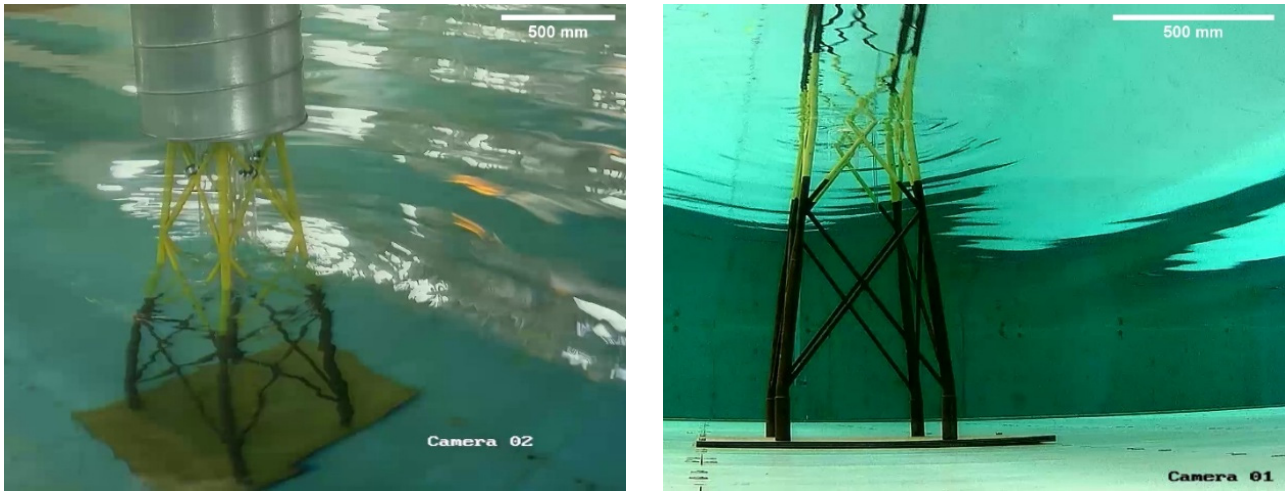

(**a**) (**b**)

Figure 2. Images of the model during tests: (**a**) the experimental set-up view; and (**b**) the model's view from an underwater camera.

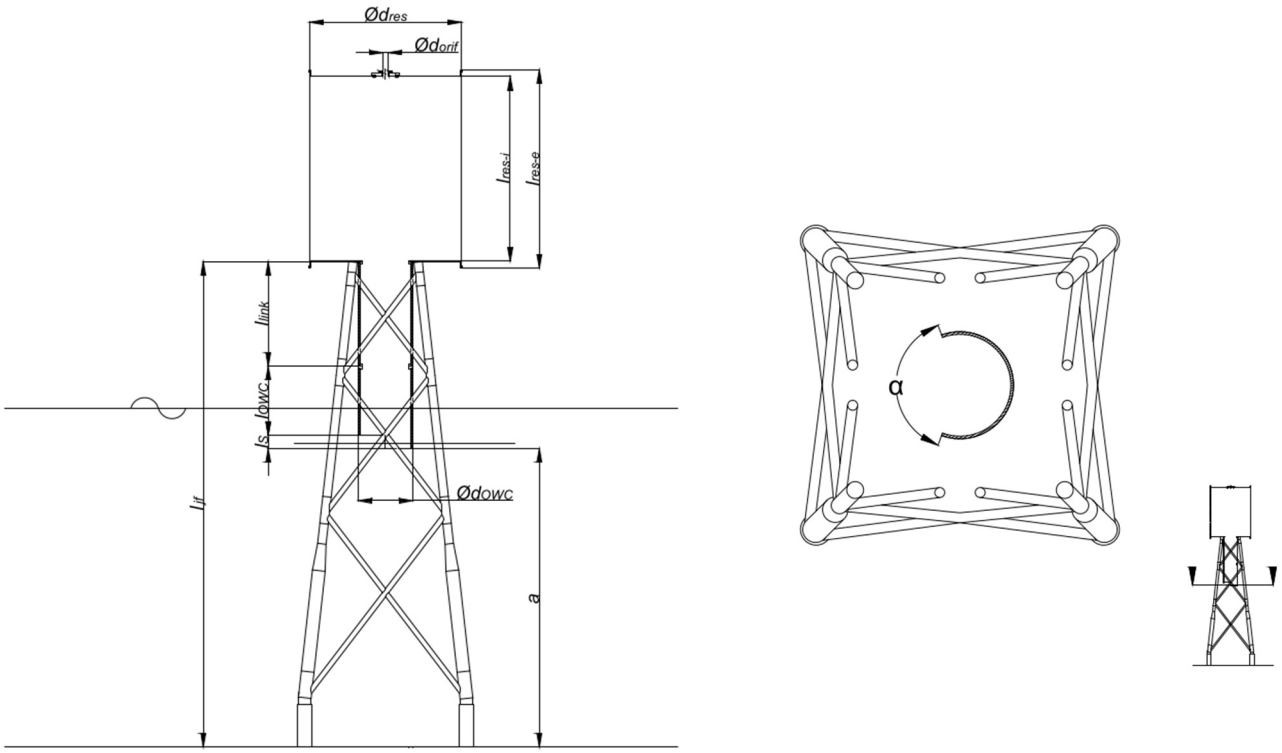

(**a**) (**b**)

Figure 3. The 1:50 scale model: (**a**) a cross-sectional view; and (**b**) a cut view displaying a horizontal plane at the skirt level (partially reproduced from [47]).

Clear acrylic pipe was used to build the four bottom sections of the OWC chamber, including the skirt. Therefore, a bottom part of the model was manufactured for each of the three skirt aperture angles and a fourth one was built without the skirt. The remainder of the model was kept as in the previous research [42]. The induced damping of the power take-off (PTO) system on the OWC at full-scale was simulated by means of an orifice plate [54,55], selecting the diameter of the orifice to match a value of the area coefficient of 1% (i.e., 15 mm) [56].

Table 1. Model main parameters.

Parameter	Symbol	Dimension
OWC air part external diameter	d_{res}	450 mm
OWC air part external length	l_{res-e}	585 mm
OWC air part internal length	l_{res-i}	545 mm
OWC air part wall-thickness	e_{res}	1.5 mm
OWC chamber draught	c	80 mm
OWC chamber external diameter	d_{OWC}	160 mm
OWC chamber length	l_{OWC}	200 mm
OWC chamber-reservoir link length	l_{link}	294 mm
OWC chamber wall-thickness	e_{OWC}	4 mm
OWC orifice diameter	d_{Orif}	15 mm
Jacket-frame length	l_{jf}	1438 mm
Jacket-frame base width	w_{jf}	525 mm
Skirt length	l_S	40 mm
Skirt angle	α	140-180-220 deg
Distance to the floor	a	884 mm
Water depth	H	1000 mm

2.2. Experimental Set-Up and Testing Programme

The characterization of the influence of the skirt angle aperture on the performance of the hybrid wind-wave energy converter was carried out through an experimental campaign at the University of Plymouth's COAST Laboratory, in the ocean basin. This is a 35 m long and 15.5 m wide basin, with a variable floor depth, which was set to match the water depth at the Wave Hub site (1.0 m at the model scale), the North Cornwall test center that was used as reference to set the metocean conditions.

Figure 4 shows the layout of the experimental set-up, including the position of the wave gauges, used to record the free surface displacement along the wave basin, and the hybrid model. Table 2 provides additional details on the exact location of the wave gauges and the model. The analysis of incident and reflected waves in the incoming wave field was conducted using the three front wave gauges (WG1, WG2, and WG3), while the rear wave gauge (WG4) recorded the transmitted wave. Additionally, a differential pressure transducer (Omega PX2300-0.5BDI, Omega Engineering Inc., Manchester, UK) tracked the pneumatic pressure difference at the OWC chamber. A sample rate of 128 Hz was set for the data acquisition.

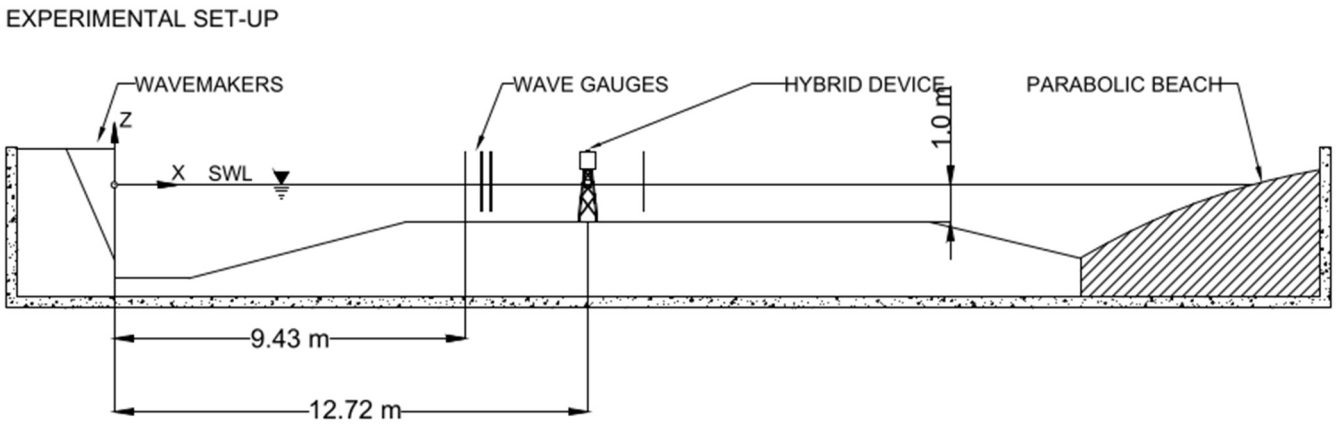

Figure 4. The experimental set-up from a side-view (partially reproduced from [47]).

Table 2. Position of model and the wave gauges (WG).

Parameter	X [m]
WG1	9.430
WG2	9.870
WG3	10.120
WG4	14.100
WG5 (OWC)	12.590
Centre of the model	12.720

A total of 47 wave conditions were used for this experimental campaign. Following [57], three different experimental test series were defined. Table 3 presents the regular waves experimental programme (referend as Series A). Meanwhile, irregular waves experimental programmes are detailed in Table 4 (referred as Series B and Series C). The duration of the tests for Series A was defined for a minimum of 100 waves, while ensuring a minimum of 60 min at prototype scale for the irregular waves test series, following [58], covering between 271 and 571 waves.

Table 3. Wave conditions for regular waves (wave period T and height H data in prototype values).

Series A		T [s]						
		6	7	8	9	10	11	12
H [m]	1.5	SA01	SA06	SA11	SA16	SA21	SA26	SA31
	2.5	SA02	SA07	SA12	SA17	SA22	SA27	SA32
	3.5	SA03	SA08	SA13	SA18	SA23	SA28	SA33
	4.5	SA04	SA09	SA14	SA19	SA24	SA29	SA34
	5.5	SA05	SA10	SA15	SA20	SA25	SA30	SA35

Table 4. Wave conditions for Series B and C, irregular waves (significant wave height H_S and energy T_E, mean T_Z and peak T_P wave period data in prototype values).

Series	Test Number	H_S	T_E	T_Z	T_P
Series B	SB01	0.5 m	6.05 s	5.04 s	7.06 s
	SB02	1.5 m	6.49 s	5.41 s	7.57 s
	SB03	2.5 m	6.98 s	5.82 s	8.14 s
	SB04	3.5 m	8.00 s	6.67 s	9.33 s
	SB05	4.5 m	8.48 s	7.05 s	9.87 s
	SB06	5.5 m	9.10 s	7.58 s	10.62 s
Series C	SC01	3.5 m	6.60 s	5.50 s	7.70 s
	SC02		7.20 s	6.00 s	8.40 s
	SC03		8.40 s	7.00 s	9.80 s
	SC04		9.00 s	7.50 s	10.50 s
	SC05		9.60 s	8.00 s	11.20 s
	SC06		11.40 s	9.50 s	13.30 s

The accuracy of the experimental set-up was ensured by means of a repeatability test series, considering both regular and irregular waves. Four different wave conditions were tested for regular waves, and two sea states were selected in the case of irregular waves. Each one of the tests was repeated four times and data from the wave gauges, the inner free surface oscillation inside the OWC chamber, and the pneumatic pressure were compared by means of the cross-correlation coefficient (R^2) and the normalised root mean square error ($NRMSE$). Table 5 shows the mean values of both statistical indicators.

Table 5. Mean values of the main statistical indicators of the repeatability tests series.

		WG1	WG2	WG3	WG4	OWC	Δp
Regular waves	R^2	0.996	0.996	0.996	0.995	0.996	0.965
	NRMSE	3.30%	3.04%	2.96%	3.27%	3.68%	5.10%
Irregular waves	R^2	0.972	0.971	0.971	0.957	0.957	0.951
	NRMSE	3.28%	3.69%	3.38%	4.55%	4.18%	3.70%

3. Results

3.1. Reflection and Transmission Analysis

Signals recorded from the wave gauges (WG1, WG2, and WG3) were analysed following the method proposed by [59,60] in order to derive the incident and reflected wave data. Furthermore, data from WG4 were also used to determine the transmitted wave. Therefore, by establishing the heights of incident, reflected, and transmitted waves, Equations (2) and (3) were applied for regular waves, while Equations (4) and (5) were utilized for irregular waves, enabling the calculation of reflection and transmission coefficients (K_R and K_T).

$$K_R = \frac{H_R}{H_I}, \tag{2}$$

$$K_T = \frac{H_T}{H_I}, \tag{3}$$

$$K_R = \sqrt{\frac{m_{0R}}{m_{0I}}}, \tag{4}$$

$$K_T = \sqrt{\frac{m_{0T}}{m_{0I}}}, \tag{5}$$

where, H_R, H_I, and H_T refer to the reflected, incident, and transmitted wave height, respectively, and m_{0i} is the generic zero order moment,

$$S_i = \int_{f_{min}}^{f_{max}} S_i(f)df, \tag{6}$$

where, S_i is the generic power spectral density.

Figure 5 illustrates regular waves data (Series A) and the four skirt angle configurations plotted against the non-dimensional wave number (kh). Transmission and reflection coefficients data obtained for irregular waves (Series B and Series C) are represented for the four skirt configurations in Figures 6 and 7, respectively. Note that the dataset containing the data from this and the remaining sections can be found in the Supplementary Materials.

It is clear from the results plotted in the figures that neither reflection nor transmission coefficients (K_R and K_T) are affected by the variation of the aperture angle. Therefore, the interaction of the device and the wave field is independent of the variation of the skirt angle. K_R increases, in general, with kh, and so decreases with the wave period for both random and regular waves, ranging from around 0.07 to 0.38 for regular waves and between 0.13 and 0.50 for irregular waves. K_T values are shown to be approximately constant at around 0.36 for regular waves, while the transmission coefficient is clearly increasing with kh for random waves, ranging from 0.06 to 0.41. This behaviour is consistent with that previously observed in [47].

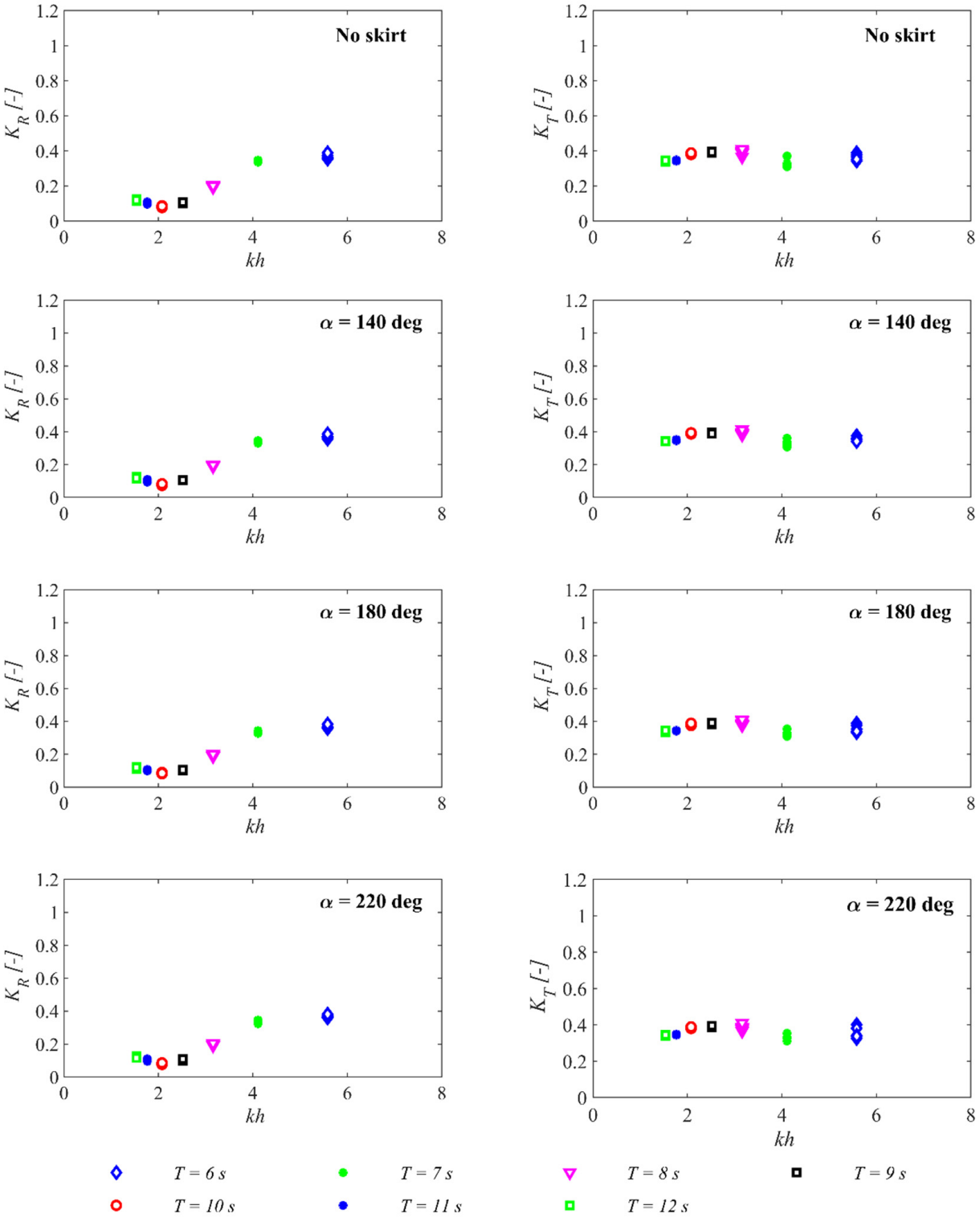

Figure 5. Values of K_R and K_T for the model with and without skirt and tree different skirt aperture angles for regular waves); (data in prototype values).

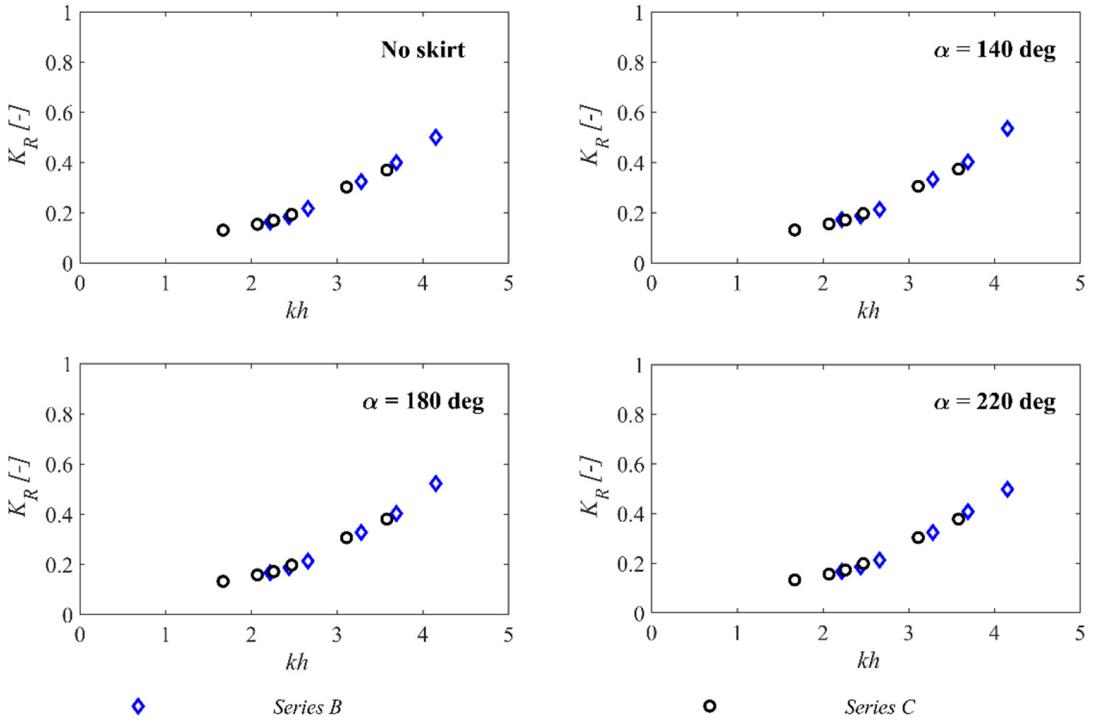

Figure 6. Values of K_R for the model with and without skirt and three different skirt aperture angles for irregular waves; (data in prototype values).

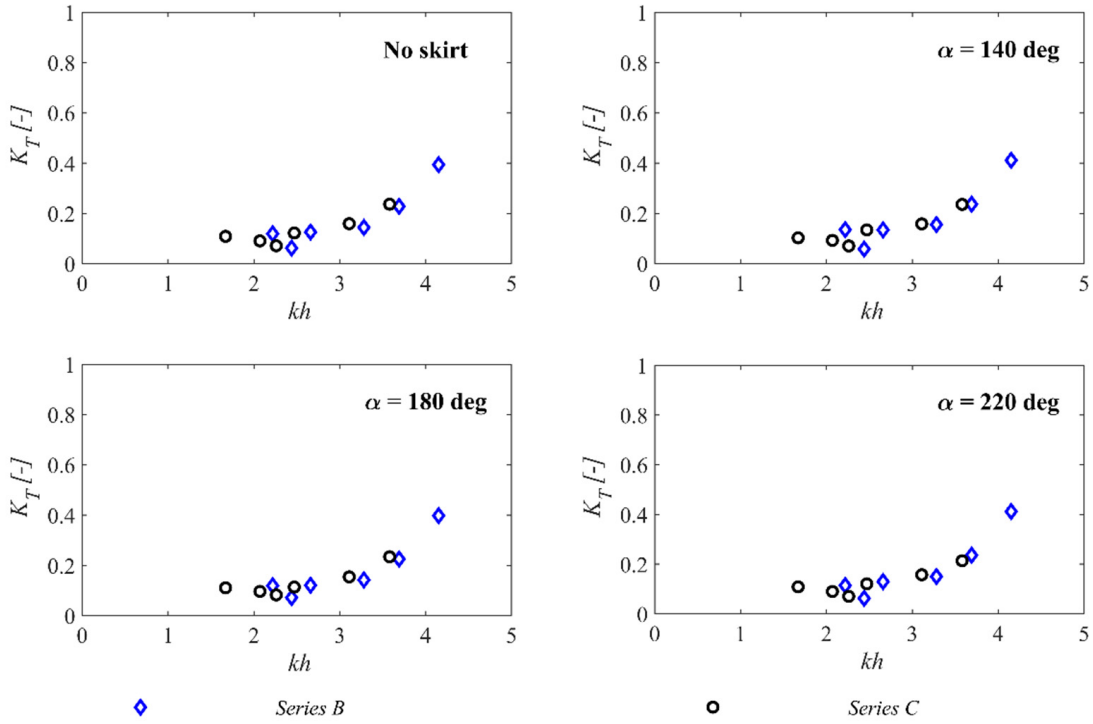

Figure 7. Values of K_T for the model with and without skirt and tree different skirt aperture angles for irregular waves; (data in prototype values).

3.2. Hybrid Wind-Wave Device Performance

The performance of the hybrid wind-wave device can be determined based on the incident wave height obtained from the reflection analysis, described in the section above, and on the data from the free surface oscillation inside the OWC chamber (WG5) and the

differential pneumatic pressure between the inner OWC chamber and the atmosphere (Δp). The performance of the device can be then evaluated by using the capture-width ratio (C_{WR}) as defined in Equation (7).

$$C_{WR} = \frac{P_m}{P\,b}, \tag{7}$$

where, P_m is the mean pneumatic power of the OWC chamber defined by Equation (8), P denotes the incident wave power per meter of wave front defined by (9) for regular wave and (10) for random ones, and b is the OWC chamber width.

$$P_m = \frac{1}{t_{max}} \int_0^{t_{max}} \Delta p\, q\, dt \tag{8}$$

where, q is the volumetric air flow rate through the chamber's orifice, t is time, and t_{max} is the time that corresponds to the duration of the test.

$$P = \frac{\rho_W\, g\, H_I^2\, c_g}{8} \tag{9}$$

$$P = \rho_W\, g \sum_{i=1}^{N} S_i(c_g)_i \Delta f \tag{10}$$

where, ρ_W is the density of the water, g stands for the acceleration of the gravity, c_g is the group velocity, H_I is incident wave height, N is the number of frequency components (for each frequency differential Δf), and S_i is the spectral density for the i-th component.

Capture-width ratio values are represented against the non-dimensional wave number (kh), first for regular waves in Figure 8 and then for irregular waves in Figure 9. Overall, C_{WR} data range from 0.5% to 7.0% for regular waves and from 1.2% to 5.4% for irregular waves. Mean values of the C_{WR} are 2.6%, 3.1%, 2.2%, and 2.9%, respectively, for angles of 0-, 140-, 180-, and 220-degrees skirt aperture for regular waves and are, respectively, 2.3%, 3.6%, 2.8%, and 2.8% for random waves.

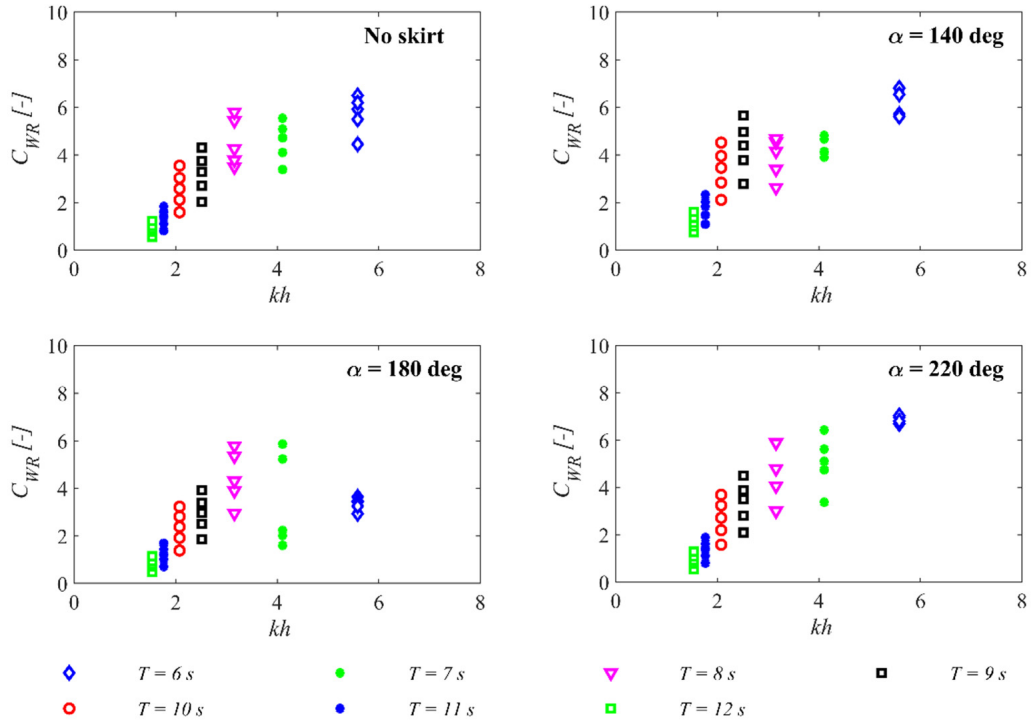

Figure 8. Values of the capture width ratio (C_{WR}) for the model with and without skirt and three different skirt aperture angles for regular waves, and for different values of the wave period (T); (data in prototype values).

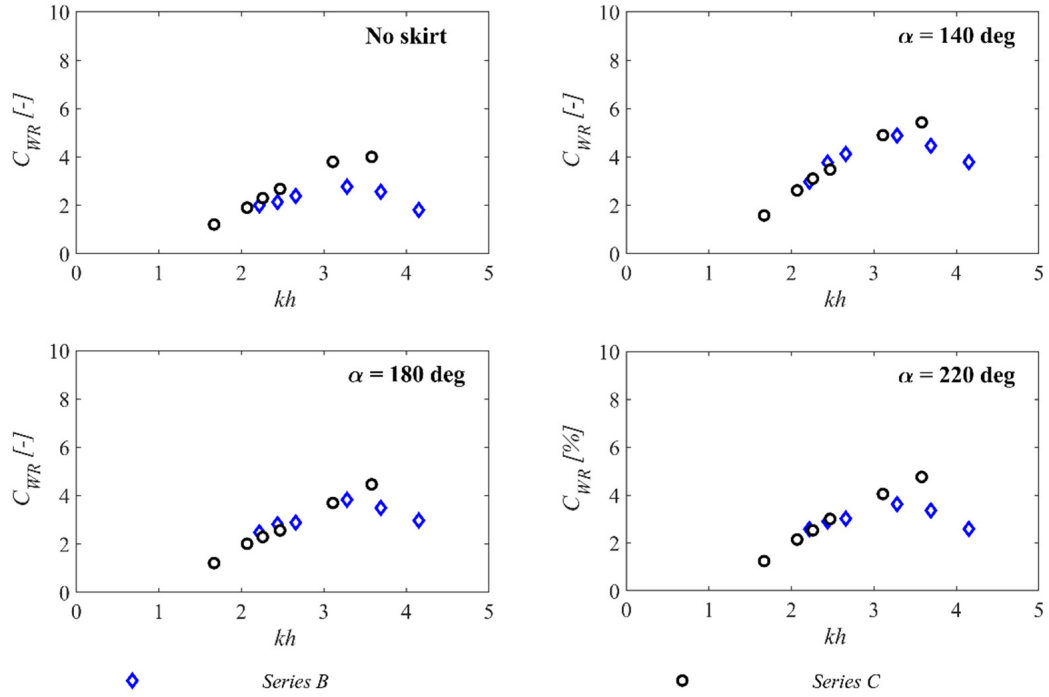

Figure 9. Values of the capture width ratio (C_{WR}) for the model with and without skirt and tree different skirt aperture angles for irregular waves; (data in prototype values).

It is clear from Figures 8 and 9 that the C_{WR} is significantly influenced by the skirt aperture angle. Though the maximum performance is found for the largest aperture, 7.0% at $\alpha = 220$ deg, the device with the smallest skirt aperture, $\alpha = 140$ deg, presents not only the best mean performance (3.1%) but also a broader area of heightened efficiency. Moreover, data from regular waves (Figure 8) and irregular waves (Figure 9) highlight the significant influence of the wave period on device performance. Generally, the C_{WR} tends to increase as the wave period decreases. From the regular waves data, different performance peaks can be identified that clearly change for each aperture angle. For the chamber without a skirt, the best performance is found at the wave periods of T = 8 and 6 s, whereas for the 140-degrees aperture angle this is found at T = 9 and 6 s; for the 180-degrees aperture angle this is found at T = 8 and 7 s, and for the 220-degrees aperture angle this is found at T = 6 s.

To delve deeper into how wave height influences the device's performance across various skirt aperture angles, as hinted in Figure 8, the capture-width matrix is defined for regular waves in Figure 10 for each of the three skirt aperture angles alongside the device configuration without a skirt. The different skirt aperture angles notably impact the optimal performance regions observed within each of the four OWC chamber configurations, showing the largest area for the aperture angle of 140-degrees, the second largest area for the angle of 220-degrees, then for the configuration without skirt and finally the smallest area is shown for the 180-degrees configuration. Furthermore, it can be observed that the increase in wave height, generally, implies an increase in the device performance.

Finally, the power matrix for regular waves is presented in Figure 11 in terms of the wave height (H) and period (T) for each one of the three skirt aperture angles and the device configuration without a skirt. The figure shows that the largest mean pneumatic power (P_m) is found at the wave period of T = 11 s.

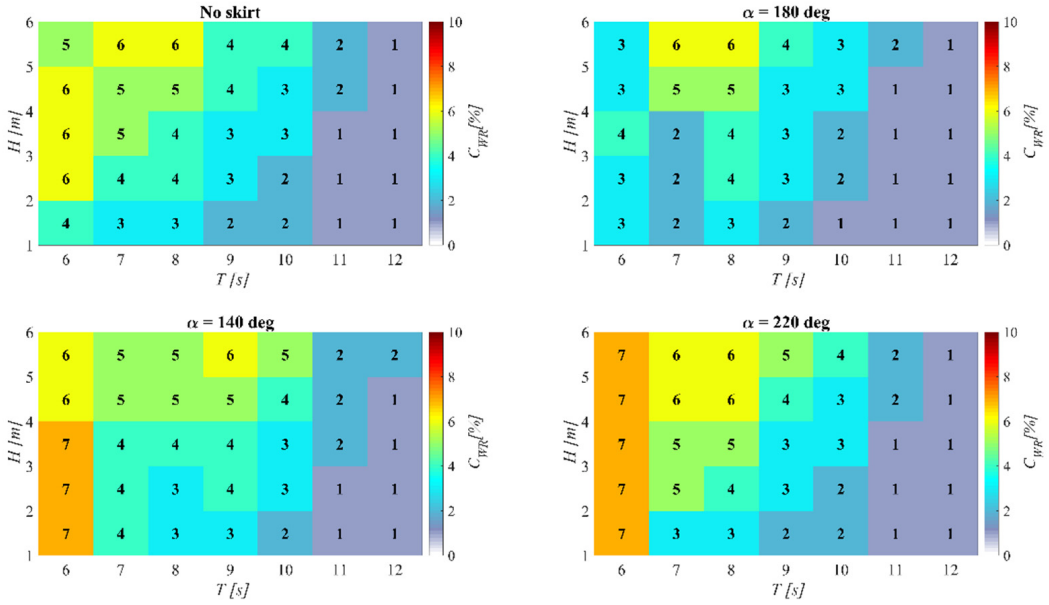

Figure 10. Capture width ratio (C_{WR}) matrices for the model with and without skirt and three different skirt aperture angles, the wave height (H) and period (T) for regular waves; (data in prototype values).

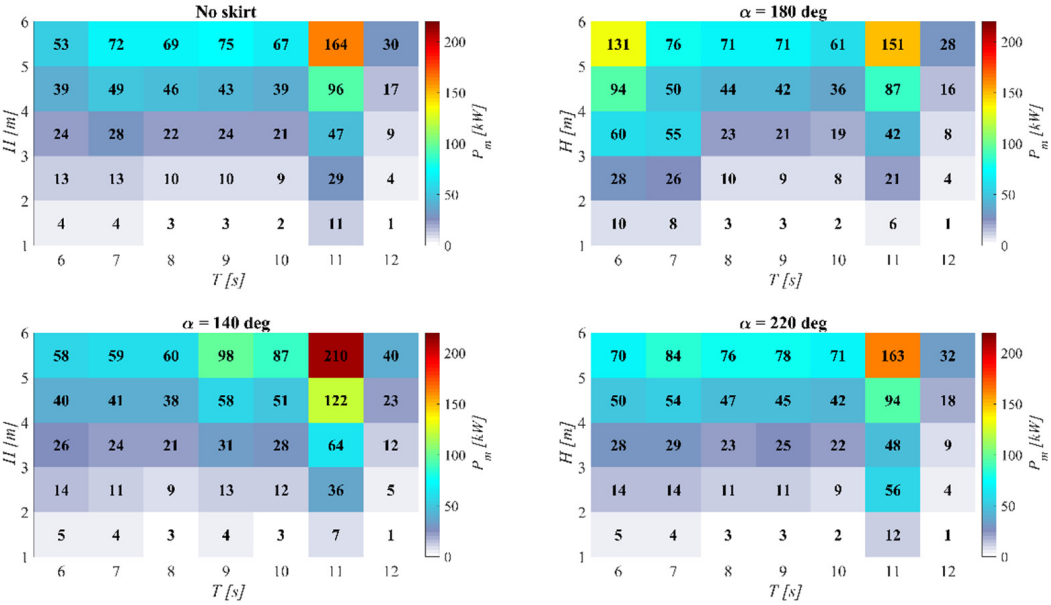

Figure 11. Power matrices for the model and its different skirt configuration, representing the mean pneumatic power for the different regular wave conditions, (data in prototype values).

4. Discussion

In this work, a novel variable aperture skirt system for an OWC WEC was studied when this was mouthed as a hybrid wind-wave energy converter on a jacket-frame offshore wind substructure system. A physical modelling test campaign was carried out on a 1:50 model of a geometrically scaled version of a jacket-frame prototype for a 50 m water depth site. In order to ensure the full-scale application of the experimental data, best practices were following when defining the experimental set-up. For example, by modifying the pneumatic part of the OWC chamber so that air compressibility effects on the aerodynamical damping are considered, the performance of the device is not overestimated. In addition to this, repeatability tests were conducted to estimate the uncertainty on the data.

The effect of the OWC's skirt aperture angle was parametrically studied by defining four different configurations of the hybrid wind-wave device, one chamber with three different exchangeable skirts, each one with a different aperture angle from a smaller to a larger aperture angle (α = 140 degree, 180 degree and 220 degree respectively). In addition, and in order to set a reference, a chamber without skirt was also tested. From the experimental data, it was observed that changes on the skirt configuration were not modifying the interaction between the hybrid device and the wave field, i.e., differences on the reflected and transmitted waves were neglectable for the four model configurations. Furthermore, regarding the device performance, a clear influence of the skirt was observed, identifying the smaller aperture angle ($\alpha = 140^{\circ}$) as the best performing one, especially for the larger wave periods (T = 9 to 12 s). This behaviour is observed for both the capture width ratio (C_{WR}) and the mean pneumatic power (P_m). It is worth remarking that the larger aperture angle configuration ($\alpha = 220^{\circ}$) has shown the best performance for the shorter wave periods (T = 6 to 8 s).

A straightforward comparison exercise will be to compare the capture width matrices of the model with the three skirt aperture angles, element by element, with the reference model without skirt. Doing this, it can be appreciated that, on average, the best performing skirt aperture angle ($\alpha = 140^{\circ}$) increases the efficiency of the OWC by about 13%. One of the characteristics defined by the patent of the skirt systems allows it to self-adapt its aperture angle to better perform for the different wave conditions. Considering this would mean that the device would select the best performing skirt configuration for each incident wave condition. Applying this optimisation to the cases tested in this research would mean that, on average, the variable skirt aperture OWC chamber would increase its efficiency by about 20%, 7% more than the best performing fix-aperture skirt. This increase in performance justifies the use of variable aperture skirt systems on isolated offshore OWC systems.

The results obtained in this research show that multipurpose platforms have a potential to coexist under jacket-frame offshore wind substructure systems. This is especially important as this type of substructure is aimed to be the leading one on the upcoming years, as the industry is moving towards deeper waters. Although it is true that the rated power of the offshore wind turbine is about two orders of magnitude larger than the OWC one (15 to 0.2 MW), when it comes time to analyse the temporal distribution of the energy yield, wave energy production is, generally, delayed and has a lower variability [61]. However, for multipurpose platforms to become a reality, there are still plenty of challenges to address; for example, the structural response of the substructure including the OWC system requires to be further studied, as well as the integration of the OWC generated energy with the offshore wind electric grid.

5. Conclusions

This work further develops a hybrid wind-wave energy converter. In particular, the research carried out here increases the understanding of a particular characteristic of this hybrid device: its variable aperture skirt angle. On the basis of the results obtained from the experimental campaign, two main outcomes can be drawn. First, the four different OWC chamber configurations tested have been shown to produce a negligible effect on both on the wave reflection and on the wave transmission. Then, it was found that the skirt aperture angle of 140-degrees was found to exhibit the best performance in terms of capture width ratio.

Based on the analysis of the performance of the hybrid wind-wave energy converter, the following main conclusions may be drawn:

- The OWC skirt aperture angle configuration was shown to not influence the wave field, meaning that the change in the skirt configuration would influence it.
- The hybrid device reflects between 7% and 50% of the incident waves, while between 6% and 41% is transmitted. It was also found that these values are similar to other WECs and hybrid devices.

- The energy conversion performance of the OWC was improved with a skirt in comparison with that of the device without a skirt.
- The best performance of the hybrid device in terms of capture width ratio occurs for the skirt aperture angle of 140-degrees.
- The region of best performance in the capture-width matrix varies in size significantly with the skirt aperture configuration, with the largest area observed for the 140-degrees aperture angle.

In summary, the variable skirt aperture angle for the jacket-frame mounted OWC hybrid device developed in this work represents a viable approach to increasing performance of OWC devices mounted as hybrid wind-wave energy converters. This work contributes to better understanding the effects of a variable aperture skirt on an OWC device. Further work is required to better understand the implementation of this kind of skirt system in OWC design.

Supplementary Materials: The following supporting information can be downloaded at: https://www.mdpi.com/article/10.3390/jmse11122383/s1.

Author Contributions: Conceptualization, C.P.-C., D.M.G. and G.I.; methodology, C.P.-C., D.M.G. and G.I.; formal analysis, C.P.-C., D.M.G. and G.I.; writing—original draft preparation, C.P.-C.; writing—review and editing, G.I. and D.M.G.; supervision, D.M.G. and G.I.; project administration, C.P.-C.; funding acquisition, D.M.G. All authors have read and agreed to the published version of the manuscript.

Funding: This research was funded by the Higher Education Innovation Fund (HEIF) and the School of Engineering, Computing and Mathematics of the University of Plymouth.

Informed Consent Statement: Not applicable.

Data Availability Statement: The research materials supporting this publication may be accessed at http://-Note: hyperlink will be added once the manuscript is accepted for publication. If you have any question regarding these research materials, please contact the corresponding author of this paper.

Acknowledgments: The authors are grateful to the COAST Lab technical support staff for their help during the experimental campaign. In addition, the authors are also grateful to Johan Skanberg-Tippen, Tim Hatton and James Harvey for all their help during the construction of the model used in this experimental campaign.

Conflicts of Interest: The authors declare no conflict of interest. The funders had no role in the design of the study; in the collection, analyses, or interpretation of data; in the writing of the manuscript, or in the decision to publish the results.

References

1. Weisse, R.; von Storch, H.; Callies, U.; Chrastansky, A.; Feser, F.; Grabemann, I.; Günther, H.; Pluess, A.; Stoye, T.; Tellkamp, J.; et al. Regional Meteorological–Marine Reanalyses and Climate Change Projections. *Bull. Am. Meteorol. Soc.* **2009**, *90*, 849–860. [CrossRef]
2. Kang, J.-N.; Wei, Y.-M.; Liu, L.-C.; Han, R.; Yu, B.-Y.; Wang, J.-W. Energy Systems for Climate Change Mitigation: A Systematic Review. *Appl. Energy* **2020**, *263*, 114602. [CrossRef]
3. Sun, X.; Huang, D.; Wu, G. The Current State of Offshore Wind Energy Technology Development. *Energy* **2012**, *41*, 298–312. [CrossRef]
4. United Nations. Framework Convention on Climate Change Adoption of the Paris Agreement. In Proceedings of the 21st Conference of the Parties, Paris, France, 30 November–13 December 2015.
5. Jeffrey, H.; Sedgwick, J. *ORECCA European Offshore Renewable Energy Roadmap*; ORECCA: Munchen, Germany, 2011; pp. 1–201.
6. Astariz, S.; Perez-Collazo, C.; Abanades, J.; Iglesias, G. Co-Located Wave-Wind Farms: Economic Assessment as a Function of Layout. *Renew. Energy* **2015**, *83*, 837–849. [CrossRef]
7. Stuiver, M.; Soma, K.; Koundouri, P.; van den Burg, S.; Gerritsen, A.; Harkamp, T.; Dalsgaard, N.; Zagonari, F.; Guanche, R.; Schouten, J.J.; et al. The Governance of Multi-Use Platforms at Sea for Energy Production and Aquaculture: Challenges for Policy Makers in European Seas. *Sustainability* **2016**, *8*, 333. [CrossRef]
8. Quevedo, E.; Delory, M.; Castro, A.; Llinas, O.; de Lara, J.; Papandroulakis, N.; Anasrasiadis, P.; Bard, J.; Jeffrey, H.; Ingram, D.; et al. Multi-Use Offshore Platform Configurations in the Scope of the FP7 TROPOS Project. In Proceedings of the 2013 MTS/IEEE OCEANS, Bergen, Norway, 10–14 June 2013; pp. 1–7.

9. Perez-Collazo, C.; Greaves, D.; Iglesias, G. A Review of Combined Wave and Offshore Wind Energy. *Renew. Sustain. Energy Rev.* **2015**, *42*, 141–153. [CrossRef]
10. Perez-Collazo, C.; Jakobsen, M.M.; Buckland, H.; Fernandez Chozas, J. Synergies for a Wave-Wind Energy Concept. In Proceedings of the EWEA Offshore 2013, Frankfurt, Germany, 19–21 November 2013; pp. 1–10.
11. Casale, C.; Serri, L.; Stolk, N.; Yildiz, I.; Cantù, M. Synergies, Innovative Designs and Concepts for Multipurpose Use of Conversion Platforms. In *Results of ORECCA Project—WP4*; ORECCA: Munchen, Germany, 2012; pp. 1–77.
12. Perez-Collazo, C.; Greaves, D.; Iglesias, G. Proof of Concept of a Novel Hybrid Wind-Wave Energy Converter. In Proceedings of the OMAE2018, Madrid, Spain, 17–22 June 2018; Volume 10. Ocean Renewable Energy.
13. Qu, Y.; Swales, J.K.; Hooper, T.; Austen, M.C.; Wang, X.; Papathanasopoulou, E.; Huang, J.; Yan, X. Economic Trade-Offs in Marine Resource Use between Offshore Wind Farms and Fisheries in Scottish Waters. *Energy Econ.* **2023**, *125*, 106811. [CrossRef]
14. Cordis Marina Platform. Available online: https://cordis.europa.eu/project/id/241402/es (accessed on 23 September 2022).
15. Cordis Mermaid. Available online: https://cordis.europa.eu/project/id/288710/reporting/es (accessed on 23 September 2022).
16. Cordis Orecca. Available online: https://cordis.europa.eu/project/id/241421/es (accessed on 23 September 2022).
17. Dong, X.; Li, Y.; Li, D.; Cao, F.; Jiang, X.; Shi, H. A State-of-the-Art Review of the Hybrid Wind-Wave Energy Converter. *Prog. Energy* **2022**, *4*, 042004. [CrossRef]
18. Wei, Y.; Bechlenberg, A.; van Rooij, M.; Jayawardhana, B.; Vakis, A.I. Modelling of a Wave Energy Converter Array with a Nonlinear Power Take-off System in the Frequency Domain. *Appl. Ocean Res.* **2019**, *90*, 101824. [CrossRef]
19. Baudry, V.; Babarit, A. Assessment of the Annual Energy Production of a Heaving Wave Energy Converter Sliding on the Mast of a Fixed Offshore Wind Turbine. In Proceedings of the Renewable Energy Congress XI (WREC XI), Abu Dhabi, United Arab Emirates, 25–30 September 2010.
20. Wan, L.; Gao, Z.; Moan, T.; Lugni, C. Experimental and Numerical Comparisons of Hydrodynamic Responses for a Combined Wind and Wave Energy Converter Concept under Operational Conditions. *Renew. Energy* **2016**, *93*, 87–100. [CrossRef]
21. Li, L.; Gao, Y.; Yuan, Z.; Day, S.; Hu, Z. Dynamic Response and Power Production of a Floating Integrated Wind, Wave and Tidal Energy System. *Renew. Energy* **2018**, *116*, 412–422. [CrossRef]
22. Konispoliatis, D.N.; Katsaounis, G.M.; Manolas, D.I.; Soukissian, T.H.; Polyzos, S.; Mazarakos, T.P.; Voutsinas, S.G.; Mavrakos, S.A. REFOS: A Renewable Energy Multi-Purpose Floating Offshore System. *Energies* **2021**, *14*, 3126. [CrossRef]
23. Iturrioz, A.; Sarmiento, J.; Ayllón, V.; Armesto, J.; Jurado, A.; Guanche, R.; Vidal, C.; Losada, I. *Experimental and Numerical Design of a Combined Wind-Wave Concept*; Taylor & Francis Books Ltd.: London, UK, 2016; pp. 667–673.
24. Aubault, A.; Alves, M.; Sarmento, A.J.N.A.; Roddier, D.; Peiffer, A. Modeling of an Oscillating Water Column on the Floating Foundation Windfloat. In Proceedings of the International Conference on Offshore Mechanics and Arctic Engineering, Rotterdam, The Netherlands, 19–24 June 2011; pp. 235–246.
25. Sarmiento, J.; Iturrioz, A.; Ayllón, V.; Guanche, R.; Losada, I.J. Experimental Modelling of a Multi-Use Floating Platform for Wave and Wind Energy Harvesting. *Ocean Eng.* **2019**, *173*, 761–773. [CrossRef]
26. Zhu, H.; Hu, C.; Sueyoshi, M.; Yoshida, S. Integration of a Semisubmersible Floating Wind Turbine and Wave Energy Converters: An Experimental Study on Motion Reduction. *J. Mar. Sci. Technol.* **2020**, *25*, 667–674. [CrossRef]
27. Zhou, Y.; Ning, D.; Shi, W.; Johanning, L.; Liang, D. Hydrodynamic Investigation on an OWC Wave Energy Converter Integrated into an Offshore Wind Turbine Monopile. *Coast. Eng.* **2020**, *162*, 103731. [CrossRef]
28. Cong, P.; Teng, B.; Bai, W.; Ning, D.; Liu, Y. Wave Power Absorption by an Oscillating Water Column (OWC) Device of Annular Cross-Section in a Combined Wind-Wave Energy System. *Appl. Ocean Res.* **2021**, *107*, 102499. [CrossRef]
29. Dang, T.D.; Phan, C.B.; Truong, H.V.A.; Le, C.D.; Nguyen, M.T.; Ahn, K.-K. A Study on Modeling of a Hybrid Wind Wave Energy Converter System. In Proceedings of the 2016 16th International Conference on Control, Automation and Systems (ICCAS), Gyeongju, Republic of Korea, 16–19 October 2016; pp. 182–187.
30. Chuan, Q.; Ping, J.; Wen, D. Hybrid Offshore Wind, Wave and Tidal Turbine Energy Conversion System: Structure and Electrical Interface. *Proc. CSEE* **2014**, *34*, 2013–2021.
31. Wang, X.; Zeng, X.; Li, J.; Yang, X.; Wang, H. A Review on Recent Advancements of Substructures for Offshore Wind Turbines. *Energy Convers. Manag.* **2018**, *158*, 103–119. [CrossRef]
32. Lozano-Minguez, E.; Kolios, A.J.; Brennan, F.P. Multi-Criteria Assessment of Offshore Wind Turbine Support Structures. *Renew. Energy* **2011**, *36*, 2831–2837. [CrossRef]
33. Falcão, A.F.O.; Henriques, J.C.C. Oscillating-Water-Column Wave Energy Converters and Air Turbines: A Review. *Renew. Energy* **2016**, *85*, 1391–1424. [CrossRef]
34. Falcão, A.F.O.; Henriques, J.C.C.; Gato, L.M.C. Self-Rectifying Air Turbines for Wave Energy Conversion: A Comparative Analysis. *Renew. Sustain. Energy Rev.* **2018**, *91*, 1231–1241. [CrossRef]
35. Simonetti, I.; Cappietti, L.; Elsafti, H.; Oumeraci, H. Optimization of the Geometry and the Turbine Induced Damping for Fixed Detached and Asymmetric OWC Devices: A Numerical Study. *Energy* **2017**, *139*, 1197–1209. [CrossRef]
36. Hayati, M.; Nikseresht, A.H.; Haghighi, A.T. Sequential Optimization of the Geometrical Parameters of an OWC Device Based on the Specific Wave Characteristics. *Renew. Energy* **2020**, *161*, 386–394. [CrossRef]
37. Boccotti, P. Comparison between a U-OWC and a Conventional OWC. *Ocean Eng.* **2007**, *34*, 799–805. [CrossRef]
38. Rezanejad, K.; Bhattacharjee, J.; Guedes Soares, C. Stepped Sea Bottom Effects on the Efficiency of Nearshore Oscillating Water Column Device. *Ocean Eng.* **2013**, *70*, 25–38. [CrossRef]

39. Howe, D.; Nader, J.-R. OWC WEC Integrated within a Breakwater versus Isolated: Experimental and Numerical Theoretical Study. *Int. J. Mar. Energy* **2017**, *20*, 165–182. [CrossRef]
40. Rezanejad, K.; Souto-Iglesias, A.; Guedes Soares, C. Experimental Investigation on the Hydrodynamic Performance of an L-Shaped Duct Oscillating Water Column Wave Energy Converter. *Ocean Eng.* **2019**, *173*, 388–398. [CrossRef]
41. Daniel Raj, D.; Sundar, V.; Sannasiraj, S.A. Enhancement of Hydrodynamic Performance of an Oscillating Water Column with Harbour Walls. *Renew. Energy* **2019**, *132*, 142–156. [CrossRef]
42. Gaspar, L.A.; Teixeira, P.R.F.; Didier, E. Numerical Analysis of the Performance of Two Onshore Oscillating Water Column Wave Energy Converters at Different Chamber Wall Slopes. *Ocean Eng.* **2020**, *201*, 107119. [CrossRef]
43. Zheng, S.; Zhu, G.; Simmonds, D.; Greaves, D.; Iglesias, G. Wave Power Extraction from a Tubular Structure Integrated Oscillating Water Column. *Renew. Energy* **2020**, *150*, 342–355. [CrossRef]
44. Zhou, Y.; Zhang, C.; Ning, D. Hydrodynamic Investigation of a Concentric Cylindrical OWC Wave Energy Converter. *Energies* **2018**, *11*, 985. [CrossRef]
45. Wan, C.; Yang, C.; Fang, Q.; You, Z.; Geng, J.; Wang, Y. Hydrodynamic Investigation of a Dual-Cylindrical OWC Wave Energy Converter Integrated into a Fixed Caisson Breakwater. *Energies* **2020**, *13*, 896. [CrossRef]
46. Collazo, C.P.; Rodriguez, J.G.I.; Greaves, D.; University of Plymouth. Wave Energy Capture Device. International Patent Application No. PCT/GB2016/051403, 24 November 2016.
47. Perez-Collazo, C.; Greaves, D.; Iglesias, G. A Novel Hybrid Wind-Wave Energy Converter for Jacket-Frame Substructures. *Energies* **2018**, *11*, 637. [CrossRef]
48. Hughes, S.A. *Physical Models and Laboratory Techniques in Coastal Engineering*; World Scientific Publishing Co. Pte. Ltd.: Singapore, 1993; ISBN 981-02-1540-1.
49. Sarmento, A.J.N.A.; Falcão, A.F.d.O. Wave Generation by an Oscillating Surface-Pressure and Its Applications in Wave Energy Extraction. *J. Fluid Mech.* **1985**, *150*, 467–485. [CrossRef]
50. Weber, J.W. Representation of Non-Linear Aero-Thermodynamic Effects during Small Scale Physical Modelling of OWC WECs. In Proceedings of the 7th European Wave and Tidal Energy Conference, Porto, Portugal, 11–13 September 2007; pp. 11–14.
51. Falcão, A.F.d.O.; Henriques, J.C.C. Model-Prototype Similarity of Oscillating-Water-Column Wave Energy Converters. *Int. J. Mar. Energy* **2014**, *6*, 18–34. [CrossRef]
52. Elhanafi, A.; Macfarlane, G.; Fleming, A.; Leong, Z. Scaling and Air Compressibility Effects on a Three-Dimensional Offshore Stationary OWC Wave Energy Converter. *Appl. Energy* **2017**, *189*, 1–20. [CrossRef]
53. Simonetti, I.; Cappietti, L.; Elsafti, H.; Oumeraci, H. Evaluation of Air Compressibility Effects on the Performance of Fixed OWC Wave Energy Converters Using CFD Modelling. *Renew. Energy* **2018**, *119*, 741–753. [CrossRef]
54. Morris-Thomas, M.T.; Irvin, R.J.; Thiagarajan, K.P. An Investigation into the Hydrodynamic Efficiency of an Oscillating Water Column. *J. Offshore Mech. Arct. Eng.* **2007**, *129*, 273–278. [CrossRef]
55. Dizadji, N.; Sajadian, S.E. Modeling and Optimization of the Chamber of OWC System. *Energy* **2011**, *36*, 2360–2366. [CrossRef]
56. Sheng, W.; Lewis, A.; Alcorn, R. On Wave Energy Extraction of Oscillating Water Column Device. In Proceedings of the 4th International Conference on Ocean Energy, Dublin, Ireland, 17–19 October 2012.
57. Hann, M.; Perez-Collazo, C. Chapter 7: Physical Modelling. In *Wave and Tidal Energy*; Greaves, D., Iglesias, G., Eds.; John Wiley & Sons Ltd.: West Sussex, UK, 2018; pp. 233–288. ISBN 978-1-119-01444-7.
58. Nielsen, K. Annex II Report 2003. In *Development of Recommended Practices for Testing and Evaluating Ocean Energy Systems*; IEA—Ocean Energy Systems: Lisbon, Portugal, 2003; pp. 1–62.
59. Mansard, E.P.; Funke, E.R. The Measurement of Incident and Reflected Spectra Using a Least Squares Method. In Proceedings of the International Conference on Coastal Engineering (ICCE), Sydney, Australia, 23–28 March 1980; Volume 1.
60. Baquerizo, A.; Losada, M.A.; Smith, J.M. Wave Reflection from Beaches: A Predictive Model. *J. Coast. Res.* **1998**, *14*, 291–298.
61. Fusco, F.; Nolan, G.; Ringwood, J.V. Variability Reduction through Optimal Combination of Wind/Wave Resources—An Irish Case Study. *Energy* **2010**, *35*, 314–325. [CrossRef]